

# Effect of cobalt doping on the magnetic properties of the spin-Peierls cuprate $\text{CuGeO}_3$

P. E. Anderson, J. Z. Liu, and R. N. Shelton

*Department of Physics, University of California, Davis, California 95616*

(Received 13 February 1997; revised manuscript received 26 June 1997)

The magnetization of single crystals in the system  $(\text{Cu}_{1-x}\text{Co}_x)\text{GeO}_3$  has been measured for compositions in the range  $0.000 \leq x \leq 0.0547$ . These crystals exhibit paramagnetic behavior, which has been fit with a Curie-Weiss expression to determine the effective moment ( $\mu_{\text{eff}}$ ) along the three principle crystal directions. For  $x \leq 0.0225$ , the spin-Peierls transition is apparent in the magnetization data, with the transition temperature ( $T_{\text{sp}}$ ) decreasing with increased cobalt doping. For  $x \geq 0.0204$ , an anisotropic magnetic transition occurs below 6 K, and is attributed to three-dimensional long-range antiferromagnetic ordering. When the field is directed along the  $c$  axis, spin-flop behavior is observed at a critical field [ $H_c(x, T)$ ] for temperatures less than the Néel temperature ( $T_N$ ). Due to the strong paramagnetism in this system,  $T_N$  and  $T_{\text{sp}}$  as a function of cobalt concentration were measured with single-crystal microcalorimetry. The effects of cobalt doping are discussed with respect to recent reports of Zn, Si, and Ni doping. [S0163-1829(97)03841-1]

## I. INTRODUCTION

Since the recent discovery of the spin-Peierls transition in  $\text{CuGeO}_3$  by Hase,<sup>1</sup> a good deal of research has been carried out on the pure compound, and on variations of the compound achieved through chemical substitution. Much of the research thus far has focused on confirming that the transition is a spin-Peierls transition, and that the other properties are consistent with that hypothesis. Perhaps the most intriguing property is the formation of a dimerized spin-zero ground state below the spin-Peierls transition temperature  $T_{\text{sp}}$ . The measured susceptibility falls sharply to a small temperature-independent constant value below  $T_{\text{sp}}$  which is consistent with a spin-zero singlet state. The explanation, that the singlet state arises due to stronger coupling between the two Cu ions of each dimerized pair, is further supported by the measured singlet-triplet energy gap structure, which has been confirmed by neutron scattering.<sup>2</sup>

Evidence that  $T_{\text{sp}}$  can be increased was reported by Takahashi,<sup>3</sup> who found that  $T_{\text{sp}}$  increases with increasing pressure. Detailed Raman scattering analysis by Goni<sup>4</sup> verified the increase, reporting the highest value to be  $T_{\text{sp}} = 25$  K at 3 GPa. Several additional papers report the effect of pressure on the spin-Peierls system.<sup>5-8</sup>

As is tradition, the process of doping this compound to change its properties began immediately after the initial report by Hase, and one of the motivating questions is clear: What would happen if some of the Cu spin-1/2 ions were replaced by ions with different spins? In general, doping is an effective way to study the physical properties of a system. Since the spin-Peierls transition is driven by the coupling of phonons to magnetic excitations, replacing some spins may well affect the transition.

Within a few months, the results of Zn doping were published,<sup>9</sup> followed by Ni,<sup>10-12</sup> Mg,<sup>13</sup> and Mn doping<sup>12</sup> on the Cu site. Several authors have reported results for Si doping on the Ge site.<sup>12,14-17</sup> Additionally, many substitutions were cataloged by Weiden,<sup>16</sup> including Ti on the Ge site. For the dopants studied thus far (Zn, Mg, Ni, Mn, Si), the effect of doping on the magnetic properties is qualitatively the

same. As the doping level increases,  $T_{\text{sp}}$  is suppressed. Above a certain doping level, a Néel state forms [three-dimensional (3D) long-range antiferromagnetic order] with  $T_N < T_{\text{sp}}$ , and coexists with the spin-Peierls order.<sup>18</sup> Associated with the Néel state is spin-flop behavior when the applied field is along the  $c$  axis. As the doping level is increased further, the spin-Peierls order is destroyed, and the Néel temperature reaches a relatively constant value.

Despite the fact that the results of doping have been studied for several dopants, and the results are consistent, there are several reasons to study the effects of cobalt doping as reported in this paper. The addition of spin-3/2 dopant to the  $\text{CuGeO}_3$  system not only makes a nonmagnetic ground state impossible, but also, the resulting effective moment will be distinct from the  $\text{Cu}^{2+}$  spin-1/2. If one assumes that dopants form  $S_{\text{imp}} + S_{\text{Cu}}$  spin states, the ground state for Ni doping would be spin-1/2, which is not distinct from the copper spin-1/2. Cobalt doping on the other hand would lead to a spin-1 ground state in the vicinity of the dopant.

## II. SAMPLE PREPARATION AND CHARACTERIZATION

The  $(\text{Cu}_{1-x}\text{Co}_x)\text{GeO}_3$  crystals were grown using the self flux method, with an additional 10% by mass of CuO and  $\text{Co}_3\text{O}_4$ . The charge was 10 g. The off-stoichiometric mixtures were well ground and placed in a platinum crucible. The powders were rapidly heated (300 °C/h) in air to 1180 °C. After holding at that temperature for 8.0 h, the melt was slowly cooled (2 °C/h) to 880 °C, and then rapidly cooled (300 °C/h) to less than 100 °C. Individual crystals were mechanically isolated from the melt. The nominal compositions grown include  $x = 0.000, 0.0005, 0.005, 0.010, 0.020, 0.030, 0.035, 0.040, 0.050, \text{ and } 0.080$ .

For a 2.98% cobalt single crystal, the space group was confirmed to be consistent with  $Pbmm$  using single-crystal x-ray diffraction.<sup>19</sup> The lattice constants are:  $a = 0.4796(2)$  nm,  $b = 0.8465(4)$  nm,  $c = 0.29468(2)$  nm.

A commercial wavelength dispersive electron microprobe<sup>20</sup> was used to determine the actual composition of the cobalt doped  $\text{CuGeO}_3$  crystals. Polished single crystals were

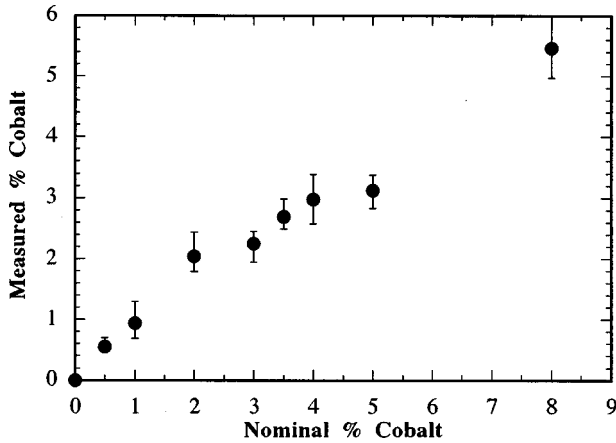


FIG. 1. The doping level as measured by electron microprobe versus the “nominal” doping level for the  $(\text{Cu}_{1-x}\text{Co}_x)\text{GeO}_3$  single crystals described in this study. The error bars indicate the range of measured values.

sampled 10–15 times along a line roughly 1 mm long. As is shown in Fig. 1, the average measured values differ from the nominal values above 2.0%. This indicates the approach to a cobalt solubility limit for the particular crystal growth technique used to produce all of the crystals discussed in this report. Higher Co doping levels might be achieved with higher peak temperatures, or by using a modified growth technique.

As will be discussed later, the cobalt doped crystals show a strong paramagnetic signal. Since the published magnetization data on Zn doped crystals<sup>21</sup> do not show this strong paramagnetic response, there are two possibilities. Either the cobalt doped crystals are not high quality (having paramagnetic impurities, crystal defects, or the cobalt ions are not substituting on the expected  $\text{Cu}^{2+}$  site) or the paramagnetism is due to the addition of cobalt ions in the copper chains. In order to eliminate the first possibility, we grew nominal 4.0% Zn crystals, to compare to published results. As with the cobalt doping, the actual doping level is less than the nominal value. The magnetization of the resultant crystals is qualitatively similar to data published for 2.0% Zn,<sup>9</sup> and electron microprobe measurements revealed the actual composition to be  $2.4\% \pm 0.4\%$  Zn. More importantly, there is not a significant paramagnetic background for the Zn-doped single crystal. These results indicate that the paramagnetic response is likely due to cobalt ions replacing copper ions, and not a crystal anomaly associated with the self-flux method used to produce the crystals for this investigation.

Polycrystalline samples were synthesized for the same range of cobalt compositions as the single crystals,  $0.00 \leq x \leq 0.050$ . Stoichiometric mixtures of  $\text{GeO}_2$ ,  $\text{CuO}$ , and  $\text{Co}_3\text{O}_4$  were well ground, pelletized, and fired twice at  $950\text{--}100^\circ\text{C}$  for at least 24 h, with an intermediate grinding.

### III. EXPERIMENT AND ANALYSIS

#### A. Magnetization

The magnetization as a function of temperature and field was measured in a commercial superconducting quantum interference device (SQUID) magnetometer.<sup>22</sup> All samples

were zero-field cooled, although no hysteresis was observed in data acquisition sequences composed of both field-cooled and zero-field-cooled measurements. Measurements of single crystal samples from each composition were made with the applied field directed along each of the three principle crystal axes, in turn. In addition, different crystals from the same melt were measured and compared, and no significant differences were found.

The molar susceptibility along the  $c$  axis as a function of temperature is shown in Fig. 2(a) for ten crystals of varying composition. The effect of cobalt doping on the magnetization data for all compositions is to add a very strong paramagnetic component. Over large ranges of magnetic field (0–55000 Oe) and temperature (2–300 K), the magnetization of these samples is directly proportional to the cobalt concentration in  $(\text{Cu}_{1-x}\text{Co}_x)\text{GeO}_3$ , for  $x < 0.0269$ . For  $x \geq 0.0269$  ( $x = 0.0269, 0.0298, 0.0313, 0.0547$  have been measured) the magnetization does not change significantly with  $x$ .

Two additional features of the susceptibility along the  $c$  axis are apparent in the data. First, the spin-Peierls transition is clearly visible at  $T \sim 14$  K for  $x \leq 0.0204$  in Fig. 2(c). Second, for  $x \geq 0.0225$ , a cusp is evident in the range  $T \sim 2\text{--}5$  K in Fig. 2(b). This cusp is not nearly so evident in the measured susceptibility along the other two crystal axes.

The magnetization at  $T = 2$  K along the  $c$  axis as a function of magnetic field is shown in Fig. 3. It is clear from the data that the saturation magnetization is affected strongly by the cobalt doping level. For  $x \geq 0.0269$ , the onset field of the spin-flop feature at  $T = 2$  K is  $H_c = 7800$  Oe. Although the data are not shown, we have found that for  $x = 0.0225$ , the spin-flop transition onset field at  $T = 1.7$  K is  $H_c = 2800$  Oe. Measurements along the other crystal directions in all cases do not show this feature, as expected.

$M$  versus  $H$  of 2.98% sample was measured along the  $c$  axis for several temperatures between 2 and 5 K, as shown in Fig. 4. The data show the critical field for the spin-flop transition increasing with increasing temperature, as expected.

#### B. Specific heat measurements

Due to the dominant paramagnetism in this system, it was difficult to determine the various transition temperatures from the magnetization data. Therefore, the Néel temperature and spin-Peierls transition temperature for the  $(\text{Cu}_{1-x}\text{Co}_x)\text{GeO}_3$  system were determined by single crystal microcalorimetry. The measurements were carried out using the relaxation method with a custom microcalorimeter.<sup>23</sup>

Using this technique, the total heat capacity of the sample plus the addenda is measured, and the heat capacity of the addenda is subtracted. Included in the addenda heat capacity is a small amount of grease used to link the sample thermally to the addenda. For this study, the empty addenda plus grease was not measured before measuring each sample. A small error is therefore introduced due to variations in the amount of grease used for each measurement to link the crystals thermally to the addenda. The heat capacity of each crystal was determined by subtracting from the total heat capacity, the measured heat capacity of the addenda loaded with a typical amount of grease. Thus, although there is good relative agreement among data for different cobalt compositions,

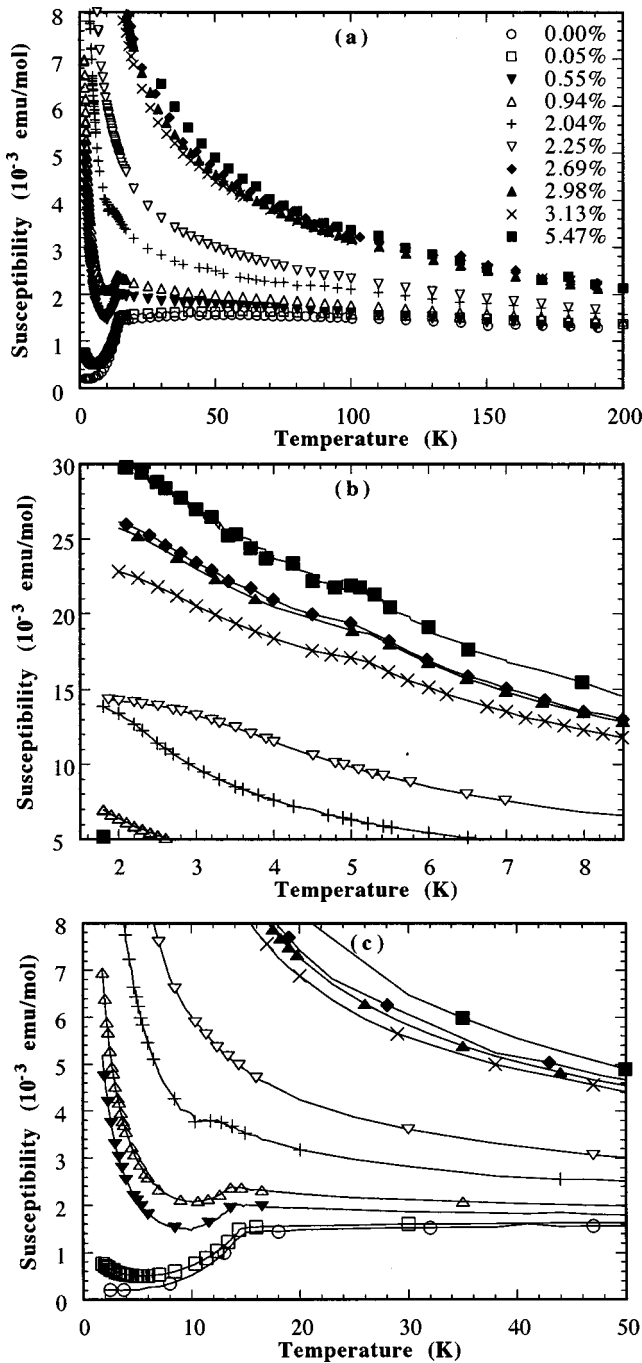


FIG. 2. The  $c$ -axis magnetic susceptibility (a) of  $(\text{Cu}_{1-x}\text{Co}_x)\text{GeO}_3$  measured with  $H=100$  Oe for various doping levels. Expanded views of the susceptibility highlight (b) a low-temperature ordering transition and (c) the spin-Peierls transition. Points have been removed to simplify the plots.

the data presented here are not intended to be quantitative; the purpose is merely to determine transition temperature. Quantitative measurements of specific heat of these compounds have been initiated.

The masses of the single crystal samples were between 1.9 and 6.5 mg. The specific heat as a function of temperature is plotted for several values of cobalt concentration in Figs. 5(a) and 5(b). It is clear that the spin-Peierls transition temperature decreases with increasing cobalt doping. The

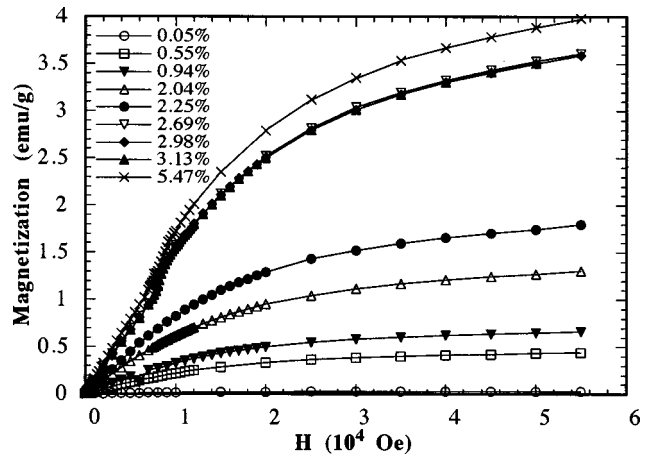


FIG. 3. The  $c$ -axis magnetization of  $(\text{Cu}_{1-x}\text{Co}_x)\text{GeO}_3$  single crystals as a function of magnetic field at  $T=2$  K. The spin-flop feature is evident for  $x \geq 0.0269$ . The  $x=0.0269$ , 0.0298, and 0.0313 data are nearly identical.

magnetic phase diagram determined from the specific heat measurements is presented in Fig. 5(c).

Three additional features of the specific heat data are worth noting. The first observation is that the spin-Peierls feature clearly decreases in magnitude and broadens with increasing cobalt concentration, especially for  $x \geq 0.0225$ . The second observation is the sharp difference between the  $x \leq 0.0225$  data and the  $x \geq 0.0269$  data. For the spin-Peierls transition, we expect an exponential component in the heat capacity below  $T_{\text{sp}}$  due to the singlet-triplet energy gap. This is clearly visible for  $x \leq 0.0225$ , but the  $x=0.0269$  and  $x=0.0298$  data look very linear all the way down to the 5.2 K ordering temperature. Lastly, the 2.69% data, as shown in Fig. 5(b), have a second low temperature peak below 2 K. This is consistent with the slight bending over of the low temperature susceptibility below about 2 K for  $x \geq 0.0269$ , as shown in Fig. 2(b).

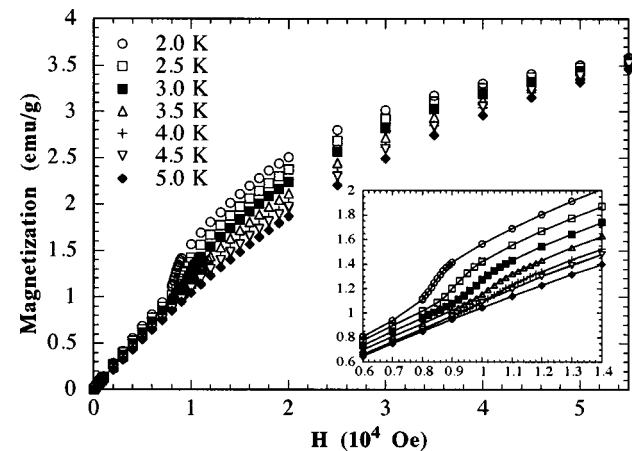


FIG. 4. The  $c$ -axis magnetization of a  $(\text{Cu}_{1-x}\text{Co}_x)\text{GeO}_3$  single crystal with  $x=0.0298$  as a function of magnetic field for several temperatures. The inset is a magnification of the 6000–14000 Oe region, showing the temperature dependence of the spin-flop critical field  $H_c$ .

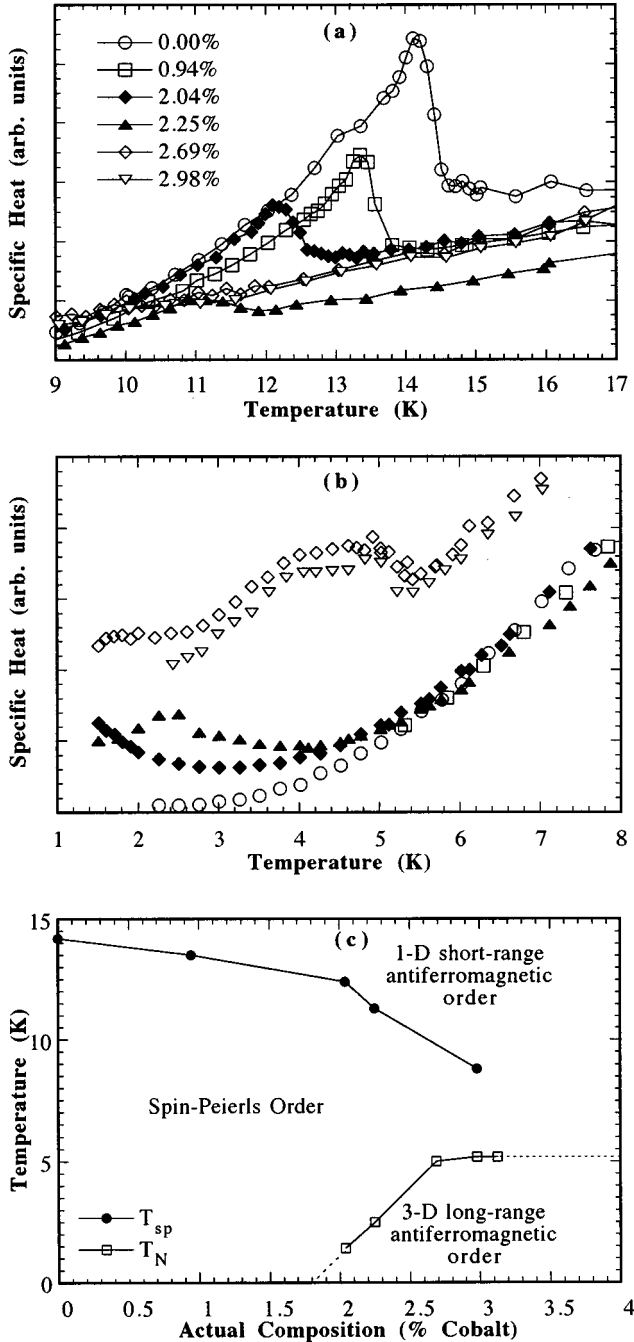


FIG. 5. The zero-field specific heat of  $(\text{Cu}_{1-x}\text{Co}_x)\text{GeO}_3$  single crystals for several cobalt concentrations. The vertical scale is not shown because the addenda specific heat was not measured before each crystal was measured. These plots highlight (a) the dependence of the spin-Peierls transition temperature on the nominal cobalt doping level, and (b) low-temperature magnetic ordering peaks. (c) is the magnetic phase diagram as determined by specific heat and magnetization measurements. The dashed lines are extrapolations.

#### IV. ANALYSIS AND DISCUSSION

##### A. Paramagnetism

The motivation behind doping the  $\text{CuGeO}_3$  system with cobalt was to investigate the effect of impurity spins on the ordered spin-Peierls state. A simplistic picture of the situa-

tion is to assume that below  $T_{sp}$ , spin impurities ( $S_{imp}$ ) dimerize with unpaired copper spins ( $S_{Cu}$ ) to form  $S_{imp} + S_{Cu}$  spin states. A statistically insignificant number of  $S_{imp} + S_{imp}$  dimers would also form. The remaining copper spins behave as spin-0 dimers below  $T_{sp}$ . If we apply this view to the cobalt spin impurities, the addition of cobalt ( $S_{imp}=3/2$ ) and copper ( $S_{Cu}=1/2$ ) spins yields  $S=1$  or 2. Since the coupling along the chain is antiferromagnetic, the  $S=1$  state would be energetically preferred. Thus, if the cobalt-doped system were consistent with the simple picture described above, the magnetic susceptibility should follow the Curie-Weiss law, with an effective moment similar to that of  $\text{Ni}^{2+}$ , which is  $S=1$ .

It is clear from Fig. 2(a) that there is a strong paramagnetic component to the measured susceptibility. Therefore, independent of any hypothesis, Curie-Weiss fits will give clues to the mechanism behind the paramagnetic behavior. However, there are several factors that restrict the temperature range over which the susceptibility can be fit with the Curie-Weiss law.

First, when fitting the data, there is no simple analytical form for the spin-Peierls transition, and this transition produces a significant kink in the low cobalt concentration ( $x < 0.023$ ) data. Even in the pure compound, the spin-Peierls transition affects the susceptibility well below  $T_{sp}$ , starting at about 5 K. This is due to thermal excitation of the triplet state. From neutron scattering results,<sup>2</sup> the energy gap between the singlet and triplet states  $\Delta E$  is 2.0 meV at 5 K, and  $k_B(5 \text{ K})=0.43 \text{ meV}$ . For  $(5 \text{ K}) \leq T \leq T_{sp}$ , the spin gap is decreasing while thermal energy increases, so the spin-1 triplet states become populated well below  $T_{sp}$ . Likewise, there is not a simple analytical form that describes the broad feature near 50 K.

Finally, Curie-Weiss fits should be done well above the ordering temperature; in this case, the Néel temperature ( $T_N$ ). Since the high-temperature data (50–300 K) cannot be fit with Curie-Weiss, we are forced to fit the data near the ordering transition. For  $x \leq 0.020$ , the ordering temperature is below 2 K. At 2 K, with  $H = 100 \text{ Oe}$ ,  $\mu H/k_B T = p_{eff}(0.0034)$ . Therefore,  $2.0 \leq T \leq 4.0 \text{ K}$  is a valid region to use Curie-Weiss for  $x \leq 0.0204$ .

The Curie-Weiss expression,

$$\chi_{\text{molar}} = \frac{C}{T - T_{\text{CW}}} + \chi_0, \quad (1)$$

$$C = \frac{\mu_B^2 N_{\text{spins}} P_{\text{eff}}^2}{3k_B},$$

was used to fit the single crystal and polycrystalline molar susceptibility data. Here,  $\chi_0$  is the temperature independent susceptibility,  $T_{\text{CW}}$  is the Curie-Weiss temperature,  $C$  is the Curie constant, and  $N_{\text{spins}}$  is the number of cobalt spins per mole, which was calculated from measured doping levels. Thus, as suggested above, we are assuming that the number of spins contributing to the observed paramagnetism in the region  $2 \leq T < 4 \text{ K}$  is equal to the number of cobalt ions in the system. The data and fits are shown in Fig. 6(a). The fit parameters for the  $c$ -axis data are shown in Table I. The fits are very stable with respect to changes in the fit range. For example, for the 0.94% Co data, extending the fit to 7 K

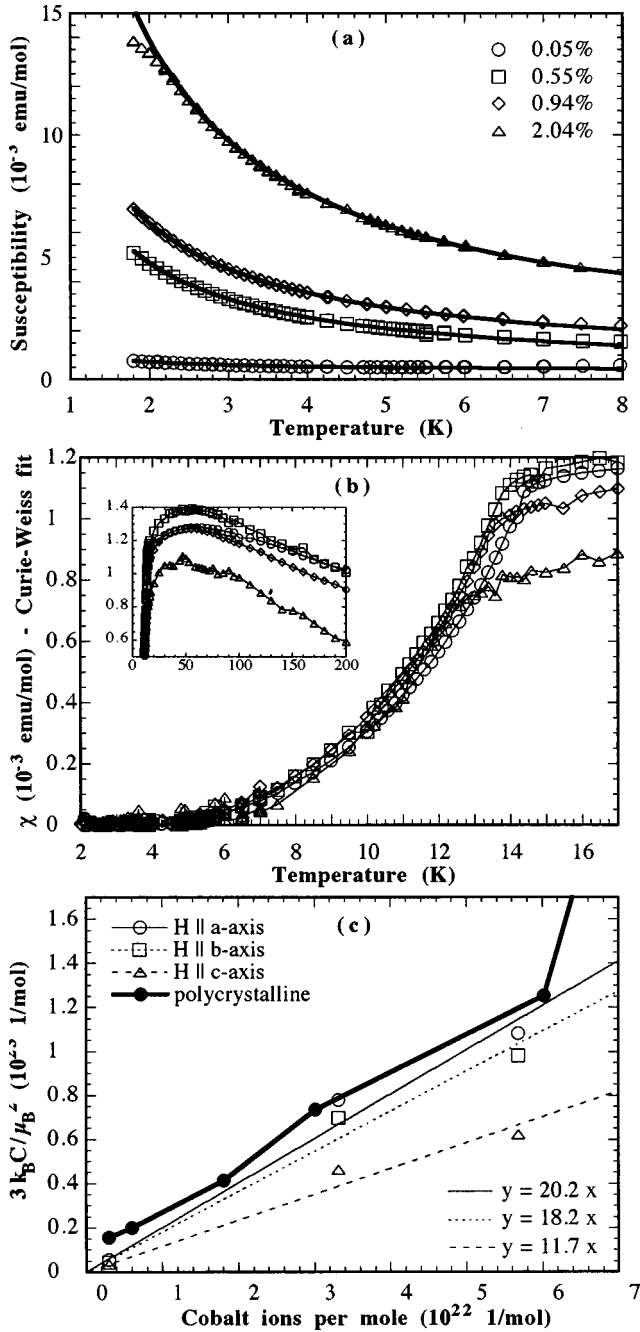


FIG. 6. The  $c$ -axis magnetic susceptibility (a) of  $(\text{Cu}_{1-x}\text{Co}_x)\text{GeO}_3$  single crystals measured with  $H=100$  Oe for various nominal doping levels, with Curie-Weiss fit, emphasizing the spin-Peierls feature. The inset shows the same subtraction at higher temperatures. (c) is a plot of  $3k_B C / \mu_B^2$  vs  $N_{\text{spins}}$  for the  $a$ -,  $b$ -, and  $c$ -axis Curie-Weiss fits to the single crystal molar susceptibility. Also shown are data for polycrystalline Curie-Weiss fits. The slope of the linear fit is the effective number of Bohr magnetons squared ( $p_{\text{eff}}^2$ ). The results are  $p_{\text{eff}}=4.5$ , 4.3, and 3.5 for the  $a$ ,  $b$ , and  $c$  axes, respectively.

reduces the Curie constant by less than 10%. In general, reasonable changes to the fit range change the Curie constant by less than 10%.

Figure 6(c) is a plot of  $3k_B C / \mu_B^2$  versus  $N_{\text{spins}}$ . As the plot shows, Curie-Weiss fits to a range of polycrystalline compositions demonstrate a dramatic upturn in the Curie

constant as a function of composition for  $x \geq 0.010$ . The single crystal data along the  $a$  and  $b$  axes also show an upturn in the Curie constant for  $x > 0.010$ . Thus linear fits to the single crystal data are restricted to  $x \leq 0.010$ . The slope of the linear fit is equal to the effective number of Bohr magnetons squared ( $p_{\text{eff}}^2$ ). The result is  $p_{\text{eff}}=3.4$  for the applied field parallel to the  $c$  axis. Representative experimentally determined values of  $p_{\text{eff}}$  for  $\text{Cu}^{2+}$ ,  $\text{Ni}^{2+}$ , and  $\text{Co}^{2+}$  are 1.9, 3.2, and 4.8, respectively.<sup>24</sup> Thus, the experimentally determined  $p_{\text{eff}}$  for this system along the  $c$  axis is closest to  $\text{Ni}^{2+}$ , a spin-1 ion. With the field along the  $a$  axis and  $b$  axis, the results are  $p_{\text{eff}}=4.5$  and 4.3, respectively, as shown in Fig. 6(c). These values are closer to the effective moment of  $\text{Co}^{2+}$ .

The difference between the effective moments along the three crystal directions is probably a result of crystal field anisotropy. The existence of a spin-flop transition along the  $c$  axis in this system is evidence of anisotropy. Additionally, for pure  $\text{CuGeO}_3$ , neutron scattering has shown that above  $T_{\text{sp}}$ , the  $\text{Cu}^{2+}$  spins are aligned along the chain,<sup>25</sup> which implies a preference for the  $c$  axis. Therefore, it is plausible that crystal field anisotropy forces unpaired copper spins to remain aligned with the  $c$  axis even when there is not long-range antiferromagnetic order.

To support the findings of the Curie-Weiss fits to  $\chi$  versus  $T$ , the magnetization versus magnetic field data were also fit. The Brillouin function [ $B_J(x)$ ] was used to fit the effective number of Bohr magnetons per cobalt ion =  $M / \mu_B N g$  versus  $x' = g \mu_B H / 2k_B T$  for  $T=2$  K along all three crystal directions. Actually, the fitting equation is  $M / \mu_B N g = (J) B_J(x')$ , and the only free parameter is the total angular momentum quantum number ( $J$ ). It was assumed that  $g=2$ , although the actual  $g$  values along the principle axes are almost certainly greater than 2, especially along the  $a$  axis. The fits were done for  $0 < H < 10000$  Oe.

One problem with the fitting is that as  $H$  increases, the spin gap between the singlet ground state and one of the triplet states decreases. Thus, singlet-triplet excitations would be expected to make a shallow-sloped contribution to the magnetization as a function of field, which reduces the quality of the Brillouin function fits. We are assuming that the nominal number of Co ions in the system is correct, and the Co ions are the main contribution to the magnetization.

The values of  $J$  along the principle axis directions obtained from the fits are shown in Table II, and are consistent with the results of the Curie-Weiss fits. The effective value of  $J$  perpendicular to the  $c$  axis is larger than the effective value of  $J$  parallel to the  $c$  axis. Generally, remembering that the  $g=2$  assumption is an underestimate of the actual  $g$  values, especially along the  $a$  axis, the Brillouin function fits indicate  $1.0 < J_{\text{cobalt}} < 1.5$ .

### B. Three-dimensional long-range antiferromagnetic order

There is another reason to fit the data with the Curie-Weiss expression. It is clear from Fig. 2(a) that the paramagnetic contribution overwhelms other magnetic behavior in this system. Subtracting the paramagnetic term will make other magnetic behavior more explicit. In particular, the spin-Peierls transition and the additional ordering peak visible in the  $x \geq 0.0225$  data.

TABLE I. The parameters associated with Curie-Weiss fits to the susceptibility for  $(\text{Cu}_{1-x}\text{Co}_x)\text{GeO}_3$  single crystals measured along the  $c$  axis. The applied field was 100 Oe.

$x$ (actual)	Fit range (K)	$C$ (emu K/mol)	$T_{\text{CW}}$ (K)	$\chi_0$ (emu/mol)
0.0005	2.0–4.0	0.00074	0.0693	$3.43e^{-4}$
0.0055	2.2–4.0	0.00958	-0.105	$2.12e^{-4}$
0.0944	2.0–4.0	0.01293	-0.182	$4.58e^{-4}$
0.0204	2.3–4.0	0.02828	-0.433	$3.22e^{-4}$

After subtracting the Curie-Weiss term from the susceptibility, several observations can be made. First, a close-up of the spin-Peierls region [Fig. 6(a)] confirms that  $T_{\text{sp}}$  decreases with cobalt doping, and that the magnitude of the spin-Peierls feature is virtually unchanged up to  $x=0.0094$ , but starts to decrease with  $x=0.0204$ . This supports the specific heat data, and implies that for  $x \geq 0.0204$ , the fraction of Cu ions that changes from spin-0 behavior to 1D antiferromagnetic ordered spins at  $T_{\text{sp}}$  is decreasing as  $x$  increases. A possible explanation for this is that some fraction of the Cu ions is not in the spin-0 state below  $T_{\text{sp}}$ . Specifically, we suggest that for  $x \geq 0.0204$ , some fraction of the Cu ions participates in 3D long range antiferromagnetic order below  $T_{\text{sp}}$ . Thus the change in susceptibility at  $T_{\text{sp}}$  will be smaller.

Second, as shown in the inset of Figs. 6(b) and 7(b), there is a broad hump in the cobalt-doped magnetization data after the Curie-Weiss contribution has been subtracted. This feature is suspiciously close to the broad  $T=50$  K hump in the undoped compound, which may be due to short-range 1D antiferromagnetic ordering.

Finally, in the low-temperature magnetization data shown in Fig. 2(b) one can see that for concentrations of 2.25%, 2.69%, 2.98%, and 3.13% cobalt, there are bumps in the magnetization at  $T=2.5$ , 5.0, 5.2, and 5.2 K, respectively.

As an example of the cobalt case, consider the 2.98% magnetization data, which are plotted along the three crystal directions in Fig. 7(a), along with a Curie-Weiss fit to the data. Although not shown, the Curie-Weiss fit extends over the temperature range 5.5–100 K, and the fit is very good. Figure 7(b) presents the same data with the Curie-Weiss fit subtracted. The subtraction shows that below 5.2 K, the  $c$ -axis magnetization is much smaller than values obtained for the other two crystal directions, and that the magnetization changes sharply at 5.2 K. This is consistent with 3D long-range antiferromagnetic ordering.

Associated with the low-temperature anisotropic transition in  $M$  versus  $T$ , which appears to be a 3D long-range

TABLE II. The effective value of  $J$ , the total angular momentum quantum number, for cobalt in  $(\text{Cu}_{1-x}\text{Co}_x)\text{GeO}_3$  with the field directed along the three principle crystallographic axes ( $J_a$ ,  $J_b$ , and  $J_c$ ) as determined from Brillouin function fits to single crystal magnetization data. The fits were done for  $0 \leq H \leq 10000$  Oe.

$x$	$J_a$	$J_b$	$J_c$
0.0005	2.00	1.54	1.27
0.0055	2.14	1.78	1.39
0.0094	1.88	1.38	1.26
0.0204	1.85	1.30	1.15
0.0225	1.85	1.40	1.30

antiferromagnetic ordering peak, there is a discontinuity in  $M$  versus  $H$  (Fig. 4) which resembles a spin-flop transition. Similar transitions have been measured for 4% Zn-doped crystals by Hase,<sup>21</sup> and 0.7% Si-doped crystals by Poirier.<sup>17</sup> With cobalt-doped crystals, the transition in  $M$  versus  $T$  occurs for  $x$  values of 0.023 and above. As noted earlier, for 2.25% Co, the initial deviation from linear  $M$  versus  $H$  occurs at about 2800 Oe for  $T=1.7$  K. For 2.69%, 2.98%, and 3.13%, the discontinuity in  $M$  vs  $H$  occurs at about 7800 Oe for  $T=2$  K. The critical field for this transition  $H_c(T, x)$  has the expected (see Appendix) temperature dependence, as shown in Fig. 4; namely, it increases as temperature is in-

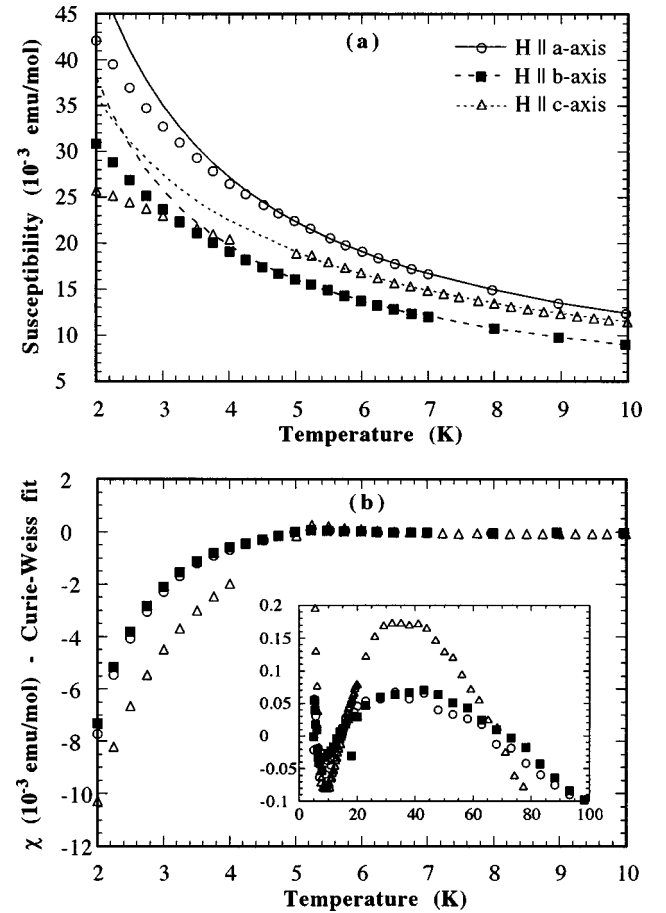


FIG. 7. The magnetic susceptibility (a) of a  $(\text{Cu}_{1-x}\text{Co}_x)\text{GeO}_3$  single crystal,  $x=0.0298$ , measured with  $H=100$  Oe along each of the three principle crystal directions, and Curie-Weiss fits to the data. The ordering peak is at  $T \sim 5.2$  K, and the fits were done over the range  $5.5 \leq T \leq 100$  K. (b) is the susceptibility along each axis minus the Curie-Weiss fit, showing the anisotropy of the ordering peak. The inset shows the same data for higher temperatures.

creased. The existence of the spin-flop transition is further proof that the low temperature ordering peak in the susceptibility corresponds to 3D long-range antiferromagnetic order.

Having established that this system order antiferromagnetically, we turn to the origin of the antiferromagnetic order. There are several indications that the Cu ions must participate in the antiferromagnetic order. Distorting the Cu chains by doping Si on the Ge site, or by replacing some ions in the Cu chain with Zn, Ni, Co, or Mn leads to antiferromagnetic order above some threshold doping level. The doping levels for which the system orders antiferromagnetically are so small that the magnetic interaction between dopant ions could not by itself lead to ordering at temperatures as high as  $T=2-5$  K. Perhaps most convincing is that the Zn doped compound orders antiferromagnetically despite the fact that Zn has no magnetic moment. Therefore, it appears that at least some fraction of the Cu ions must participate in the three-dimensional long-range antiferromagnetic order.

A plausible picture for a fraction of the Cu ions participating in the Néel state is as follows. A magnetic moment is induced in the Cu chain in the vicinity of impurities. There is a length scale associated with these regions, and once the doping level is high enough for the regions to overlap, the system orders antiferromagnetically. This picture is supported by the fact that above a certain doping concentration, the Néel temperature remains relatively constant.

There is also evidence that the dopant ions influence the antiferromagnetic order. For Zn, Co, and Mn doping, the  $c$  axis is the easy axis. However, for Ni doping, we have observed that for 2.0% Ni single crystals, the  $a$  axis is the easy axis. Thus, the ions substituted for Cu ions also play a role in the formation of the three-dimensional long-range antiferromagnetic order.

Our specific heat and magnetic susceptibility data show the existence of a second low-temperature ordering peak for  $x \geq 0.0269$ . Because the susceptibility remains strongly paramagnetic below the initial peak at 5.1 K, the Co moments may not freeze out completely until the lower ordering temperature, at  $T \sim 2.0$  K.

As a quantitative comparison of the effect of doping in the  $\text{CuGeO}_3$  system, consider Fig. 5(c), which displays  $T_N$  and  $T_{sp}$  as functions of cobalt concentration. A comparison of our results with reports of the effects of Si,<sup>14</sup> Zn,<sup>18</sup> and Ni (Ref. 10) doping indicates that doping with Si on the Ge site has the most dramatic effect on  $T_{sp}$  and leads to the formation of the Néel state much lower concentrations than doping on the Cu site with Zn, Ni, or Co. Among the three transition metal dopants, Zn has the most dramatic effect on  $T_{sp}$  and on the formation of the Néel state, while Co has the least dramatic effect. It should be pointed out that there is some disagreement in the literature at this time. However, the references cited above are consistent with magnetization measurements we have made on 2.0% Ni and 2.4% Zn single crystals. Finally, preliminary magnetization measurements on Mn-doped single crystals indicate that Mn may affect the system even less than Co.

### C. Coexistence of spin-Peierls and 3D LRAF order

The published results for Ni, Zn, and Si doping (Refs. 10, 18, and 14, respectively) indicate the coexistence of 3D long-

range antiferromagnetic order and spin-Peierls order at low temperatures. Our cobalt-doped samples exhibit similar behavior. The antiferromagnetic ordering peak is visible in the specific heat data and the susceptibility data for  $x \geq 0.0204$ . The spin-Peierls transition is also visible in the specific heat and susceptibility data for  $x \leq 0.0225$ . In addition, the  $x = 0.0269$  and  $x = 0.0298$  specific heat data show a very small, broad feature at about 8.8 K, which could correspond to the spin-Peierls transition. Whether or not there is spin-Peierls order for  $x \geq 0.0269$ , our data show the presence of both 3D long-range antiferromagnetic order and spin-Peierls order for a range of compositions. Fukuyama has shown that disorder caused by impurity doping in this system can lead to the coexistence of 3D long-range antiferromagnetic order and spin-Peierls order.<sup>26</sup> The cobalt doping levels in this study are similar to the Si and Zn doping levels discussed in his paper. More measurements are needed to determine whether the spin-Peierls transition occurs above  $x = 0.030$ , and the nature of the spin structure at various temperatures.

## V. CONCLUSIONS

We have measured the magnetization along the three principle crystal directions as a function of field and temperature for polycrystalline and single crystal  $(\text{Cu}_{1-x}\text{Co}_x)\text{GeO}_3$ , with compositions in the range  $0.000 \leq x \leq 0.055$ . Due to large paramagnetic signal in these compounds, the Néel temperature and spin-Peierls temperature were determined by single crystal microcalorimetry.

The results indicate that doping with Co on the Cu site is similar to doping with Zn, or Ni; the spin of the dopant plays little role except to add an underlying paramagnetism to the magnetization data. As in the Ni- and Zn-doped systems, increased Co doping leads to the suppression of  $T_{sp}$ , and 3D long-range antiferromagnetic order. Since the spin of the dopant plays little role in the general characteristics of the antiferromagnetic ordering—its temperature, anisotropic nature, or the spin-flop behavior—we suggest that the mechanism behind the antiferromagnetic ordering is more dependent on interrupted copper chains than on the ions that do the interrupting. However, there are clearly differences in the rate at which  $T_{sp}$  is suppressed,  $T_N$  as a function of doping concentration, and even the easy axis direction.<sup>27</sup> We have compared the effect of Co doping to Si, Zn, and Ni doping, based on data in the literature and/or on our own measurements,<sup>27</sup> and concluded that a higher concentration of Co is required to suppress  $T_{sp}$ , and to form the Néel state below  $T_{sp}$ .

We have argued that the choice of cobalt as a doping impurity provides a unique opportunity to study the spin interactions that result in a singlet ground state for the undoped system. In particular, we have suggested that in the dimerized spin-Peierls state, cobalt impurity spins have a stronger interaction with unpaired copper spins than with the neighboring copper-copper dimer, and thus form  $S_{imp} + S_{Cu}$  spin states. Our  $c$ -axis magnetization data support the hypothesis that, at low concentrations, the cobalt ions dimerize with copper ions below  $T_{sp}$  to form spin-one effective moments.

We have reported the dependence of the spin-flop critical field  $H_c$  on temperature, and it agrees with expectation. Lastly, our cobalt-doped crystals clearly demonstrate the co-

existence of spin-Peierls order and long-range antiferromagnetic order for a range of compositions.

#### ACKNOWLEDGMENTS

The authors wish to thank the National Science Foundation, Grant No. DMR-94-03895, for support for this work. Partial support to P.E.A. was provided by UC Davis. Additional thanks go to Peter Klavins for his assistance with the various measurements, and to Rajiv R.P. Singh for many helpful discussions during the course of this work.

#### APPENDIX

Neutron scattering has shown that above  $T_{sp}$  the spins are aligned along the chain,<sup>25</sup> which implies that the  $c$  axis is the easy axis. When there is a preferred crystal direction, the energy can be expressed as<sup>28</sup>

$$E = -K \cos^2(\vartheta) - \frac{1}{2} \chi_{\perp} H^2 \sin^2(\vartheta - \vartheta_H) - \frac{1}{2} \chi_{\parallel} H^2 \cos^2(\vartheta + \vartheta_H), \quad (A1)$$

where  $\vartheta_H$  is the angle between the preferred axis and the field,  $\vartheta$  is the angle between the spins and the preferred axis, and  $K$  is the anisotropy energy. Letting  $\vartheta_H = 0$ , and minimizing the energy with respect to  $\vartheta$  gives

$$H_c = \sqrt{2K/(\chi_{\perp} - \chi_{\parallel})}. \quad (A2)$$

Thus, as the Néel temperature is approached from below, the difference between perpendicular and parallel susceptibilities goes to zero, and the critical field  $H_c(T, x)$  increases.

- 
- <sup>1</sup>M. Hase, I. Terasaki, and K. Uchinokura, *Phys. Rev. Lett.* **70**, 3651 (1993).
- <sup>2</sup>O. Fujita, J. Akimitsu, M. Nishi, and K. Kakurai, *Phys. Rev. Lett.* **74**, 1677 (1995).
- <sup>3</sup>H. Takahashi, N. Mori, O. Fujita, J. Akimitsu, and T. Matsumoto, *Solid State Commun.* **95**, 817 (1995).
- <sup>4</sup>A. R. Goni, T. Zhou, U. Schwarz, R. K. Kremer, and K. Syassen, *Phys. Rev. Lett.* **77**, 1079 (1996).
- <sup>5</sup>A. Jayaraman, S. Y. Wang, L. C. Ming, and S. W. Cheong, *Phys. Rev. Lett.* **75**, 2356 (1995).
- <sup>6</sup>S. Katano, O. Fujita, J. Akimitsu, and M. Nishi, *Phys. Rev. B* **52**, 15364 (1995).
- <sup>7</sup>M. Nishi, O. Fujita, J. Akimitsu, K. Kakurai, and Y. Fujii, *Phys. Rev. B* **52**, R6959 (1995).
- <sup>8</sup>H. Yamaguchi, T. Ito, K. Oka, and H. Obara, *J. Phys. Soc. Jpn.* **62**, 3801 (1993).
- <sup>9</sup>M. Hase, I. Terasaki, Y. Sasago, K. Uchinokura, and H. Obara, *Phys. Rev. Lett.* **71**, 4059 (1993).
- <sup>10</sup>J. G. Lussier, S. M. Coad, D. F. McMorrow, and D. M. Paul, *J. Phys.: Condens. Matter* **7**, L325 (1995).
- <sup>11</sup>V. Kiryukhin and B. Keimer, *Phys. Rev. B* **52**, 704 (1995).
- <sup>12</sup>S. B. Oseroff, S. W. Cheong, B. Aktas, M. F. Hundley, Z. Fisk, and L. W. Rupp, *Phys. Rev. Lett.* **74**, 1450 (1995).
- <sup>13</sup>M. Hase, Y. Sasago, K. Uchinokura, G. Kido, and T. Hamamoto, *J. Magn. Magn. Mater.* **140**, 1691 (1995).
- <sup>14</sup>J. P. Renard, K. Le Dang, P. Veillet, G. Dhalenne, A. Revcolevschi, and L. P. Regnault, *Europhys. Lett.* **30**, 475 (1995).
- <sup>15</sup>J. P. Schoeffel, J. P. Pouget, G. Dhalenne, and A. Revcolevschi, *Phys. Rev. B* **53**, 14971 (1996).
- <sup>16</sup>M. Weiden, W. Richter, C. Geibel, F. Steglich, P. Lemmens, B. Eisener, M. Brinkmann, and G. Guentherodt, *Physica B* **225**, 177 (1996).
- <sup>17</sup>M. Poirier, R. Beaudry, M. Catonguay, M. L. Plumer, G. Quirion, F. S. Razavi, A. Revcolevschi, and G. Dhalenne, *Phys. Rev. B* **52**, R6971 (1995).
- <sup>18</sup>Y. Sasago, N. Koide, K. Uchinokura, M. C. Martin, M. Hase, K. Hirota, and G. Shirane, *Phys. Rev. B* **54**, R6835 (1996).
- <sup>19</sup>The single crystal measurements were made on a Syntex P2<sub>1</sub> four-circle x-ray diffractometer, using Cu  $K\alpha$  radiation, wavelength=0.15478 nm.
- <sup>20</sup>The measurements were made with a Cameca SX-50 electron microprobe. The parameters for the electron microprobe measurements were as follows: accelerating potential=20 keV, beam current=10 nA, rastered beam at 100 000 times magnification ( $\sim 1 \mu\text{m}$  square beam size), scanning for  $K\alpha$  lines of Cu, Co, and Ge, with ZAF matrix corrections.
- <sup>21</sup>M. Hase, N. Koide, K. Manabe, Y. Sasago, K. Uchinokura, and A. Sawa, *Physica B* **215**, 164 (1995).
- <sup>22</sup>Quantum Design Inc., 11578 Sorrento Valley Road, San Diego, CA 92121.
- <sup>23</sup>R. Bachmann, F. J. DiSalvo, T. H. Geballe, R. L. Greene, R. E. Howard, C. N. King, H. C. Kirsch, K. N. Lee, R. E. Schwall, H. U. Thomas, and R. B. Zubeck, *Rev. Sci. Instrum.* **43**, 205 (1972).
- <sup>24</sup>C. Kittel, *Introduction to Solid State Physics*, 6th ed. (Wiley, New York, 1986), p. 406.
- <sup>25</sup>M. Fujita, K. Ubukata, M. Arai, T. Tonegawa, M. Mino, M. Motokawa, K. Knight, B. Forsyth, S. M. Bennington, J. Akimitsu, and O. Fujita, *Physica B* **219**, 95 (1996).
- <sup>26</sup>H. Fukuyama, T. Tanimoto, and M. Saito, *J. Phys. Soc. Jpn.* **65**, 1182 (1996).
- <sup>27</sup>P. E. Anderson, J. Z. Liu, and R. N. Shelton (unpublished) magnetization data for Zn, Ni, and Mn single crystals.
- <sup>28</sup>S. Chikazumi, *Physics of Magnetism* (Wiley, New York, 1964), p. 135.